JOURNAL OF APPLIED ELECTROCHEMISTRY 25 (1995) 219–226

Physical and electrochemical characteristics of nickel hydroxide as a positive material for rechargeable alkaline batteries

K. WATANABE, T. KIKUOKA

Shin-Kobe Electric Machinery Co., Ltd, Shinjyuku-Mitsui Building, No. 1-1, 2-chome, Nishishinjyuku, Shinjyuku-ku, Tokyo 163, Japan

N. KUMAGAI

Department of Applied Chemistry and Molecular Science, Faculty of Engineering, Iwate University, Morioka 020, Japan

Received 1 June 1994; revised 24 September 1994

Nickel hydroxide is widely used as an active material in pasted-type nickel electrodes. Physical properties of several nickel hydroxide powders have been examined by laser diffraction, BET, X-ray diffraction, thermal analysis and SEM. Nickel hydroxide powder with a smaller crystalline size shows better charge–discharge cyclic characteristics. The chemical diffusion coefficients of the proton in the nickel hydroxide sample are measured by a current pulse relaxation method. Nickel hydroxide with a smaller crystalline size shows a higher proton diffusion coefficient, giving excellent cycling behaviour.

1. Introduction

Much interest has centred in recent years on the development of rechargeable alkaline batteries with high energy densities. To improve the cell performance, such as energy density, pasted-type nickel electrodes have been developed [1, 2]. This type of nickel electrode was fabricated by filling the pasted-type of nickel hydroxide ($Ni(OH)_2$) as an active material in a nickel foam substrate.

In the present work four kinds of nickel hydroxide powder samples with different physical properties, such as surface area, crystal form and crystalline size, were used as positive electrodes in rechargeable alkaline batteries. The electrochemical properties including charge–discharge characteristics of the four kinds of nickel hydroxide powders have been investigated and, moreover, kinetics of proton insertion into the network of nickel hydroxide have been studied using a current–pulse relaxation technique.

2. Experimental details

2.1. *Preparation of electrode materials*

As a nickel electrode substrate, nickel foam ($2 \times 2\,cm^2$, Sumitomo Electric Industries, Ltd) was used. The following four kinds of β-type nickel hydroxide (β-$Ni(OH)_2$) powders (A–D) were used as positive materials. Samples A, B and C were obtained from the Nihon Kagaku Sangyo Company and sample D was obtained from the Tanaka Chemical Corporation. Cobalt metal powder (Société Générale Métallurgique de Hoboken) was added to the hydroxides to increase the utilization of the active materials [1, 2]. Hydroxypropyl-methyl-cellulose (HPMC) (Shin-Etsu Chemical Co.) and PTFE dispersion (Daikin Industries, Ltd) were used as binders.

2.2. *Analysis of nickel hydroxide samples*

The chemical compositions of the nickel hydroxide powder samples were obtained using an inductively coupled argon plasma emission spectrophotometer (model P-5200, Hitachi Ltd). The surface area was obtained by the BET adsorption method using a surface area analyser (model MIC-2205, Micromeritics Ltd).

The particle size distribution of the hydroxide powder samples was obtained using SPA (Microtrack Ltd). Scanning electron microscope (SEM) observation was performed using an S-900 microscope (Hitachi Ltd). X-ray diffraction measurements were performed using a RINT-1100 diffractometer (Rigaku Ltd), Cu$K\alpha$ radiation and a nickel filter at 40 kV and 20 mA. Thermal analysis was carried out with a thermal analyser, model DT-40 (Shimadzu Co.).

2.3. *Preparation of nickel electrode*

10 g of each nickel hydroxide powder (samples A–D) and 0.5 g of cobalt powder were mixed in an agate mortar. Then 3.0 g of aqueous suspension containing 2.0 wt % HPMC as a binder was added to the mixed powder and mixed again. The mixture obtained was

0021-891X

incorporated in the nickel foam electrode using a spatula, and dried in air in an oven at 60 °C for 1 h. The electrode was then dipped in PTFE dispersion (5% solid in water), dried in air in an oven at 60 °C for 1 h and pressed at 420 kg cm^{-2}. The geometrical surface area of the nickel electrode was 4 cm^2 and the weight of nickel hydroxide was about 0.14 g cm^{-2}. These nickel electrodes were spot welded with 6 mm nickel ribon as a current collector.

2.4. *Electrochemical measurements*

Electrochemical measurements of the nickel electrode were performed using a glass beaker cell. A nickel mesh was used as a counter electrode, and 30 wt % KOH was used as the electrolyte. Hg/HgO (30 wt % KOH) was used as a reference electrode. The electrolysis cell was placed in an incubator held at a given temperature (± 1 °C).

Charging was initially carried out at a rate of 7.0 mA cm^{-2} for 6 h. Then discharging was carried out at the same rate down to 0.1 V vs. Hg/HgO at 20 °C, followed by a recharge at a rate of 7.0 mA cm^{-2} for 6 h. The theoretical capacity of nickel hydroxide is 289 mA h (g-active material)$^{-1}$ by assuming the electrode reaction as

$$Ni(OH)_2 + OH^- \rightleftharpoons NiOOH + H_2O + e^- \quad (1)$$

The composition of the working electrode was changed by coulometric titration. To reach equilibrium after coulometric titration required 20 to 50 h at a constant temperature in order to obtain uniform H^+ ion distribution throughout the working electrode. Equilibrium was considered to have been reached when the open-circuit voltage was stabilized to less than 0.1 mV h^{-1} at a constant temperature. The proton diffusion coefficients, $\tilde{D}$, in the hydroxides were measured using the current pulse relaxation (CPR) technique described by Basu and Worrell [3], Kumagai *et al.* [4] and Dickens *et al.* [5] using the formula for the time-dependence of the transient voltage (ΔE), i.e.

$$\Delta E = IV_m\tau(dE/dn)/FA(\pi\tilde{D}t)^{1/2} \quad (2)$$

where I is a current pulse (300 mA), V_m is the molar volume (22.61 cm^3, which was obtained by assuming the sample as β-nickel hydroxide), τ is the duration of the pulse (8 s), (dE/dn) is the slope of open circuit voltage (o.c.v.), A is the apparent geometric area (which is assumed to be true in the present work). In Expression 2 $n = 0 \sim 1$ is used by assuming the following electrode reaction:

$$Ni(OH)_2 + OH^- \rightleftharpoons NiOOH + H_2O + e^- \quad (3)$$

or

$$H_nNiOOH \rightleftharpoons NiOOH + nH^+ + ne^- \quad (4)$$

A current pulse generator (model HC-113, Hokuto Denko Ltd) was used. The resulting potential–time transients were recorded using an oscilloscope for a short duration and a voltage recorder over long durations.

Table 1. Physical properties of nickel hydroxide samples

Sample	Chemical composition			Mean diameter/μm	BET surface area/m^2 g^{-1}
	Ni/%	Co/%	Cd/%		
A	61.7	0.16	< 0.01	15	19
B	61.8	0.13	< 0.01	14	38
C	61.9	0.19	< 0.01	14	38
D	61.5	0.56	< 0.01	17	25

3. Results and discussion

3.1. *Physical properties of nickel hydroxide samples*

The chemical compositions and physical properties for nickel hydroxide samples are presented in Table 1. The nickel and cadmium contents are nearly the same in these samples, but the cobalt contents in samples A, B and C are slightly less than in sample D. The mean diameter of these samples is 14 ~ 17 μm, and BET surface areas are 19 ~ 38 m^2 g^{-1}.

The SEM photographs of the nickel hydroxide samples are shown in Fig. 1. At low magnification, the samples appear spherical, while at a higher magnification they are found to consist of many tiny crystals. Sample A consists mainly of coarse crystals, while sample B contains fine crystals. Samples C and D are made up of stacks of thin plate-like crystals.

The XRD patterns of the samples are given in Fig. 2. The full width of half maximum intensity (FWHM) of the respective samples in (0 0 1) and (1 0 1) lines are displayed in Table 2. From Fig. 2 and Table 2 the diffraction peak intensity and FWHM are different in each sample. The FWHM for sample A is the smallest, while that for sample C is the largest, showing that the crystalline size of the hydroxide powder in sample A is the largest, while that for sample C is the smallest [6].

Figure 3 shows the DTA curves of the samples. In each sample a clear endothermic peak was observed around 300 °C, due to the decomposition of the hydroxide accompanying dehydration. The decomposition temperatures for samples C and D are clearly lower than for samples A and B. This is consistent

Table 2. The FWHM values in (0 0 1) and (1 0 1) diffraction lines of nickel hydroxide samples

Sample	(2θ/deg)	
	(0 0 1)	(1 0 1)
A	0.529	0.432
B	0.708	0.554
C	1.095	1.153
D	0.712	0.879

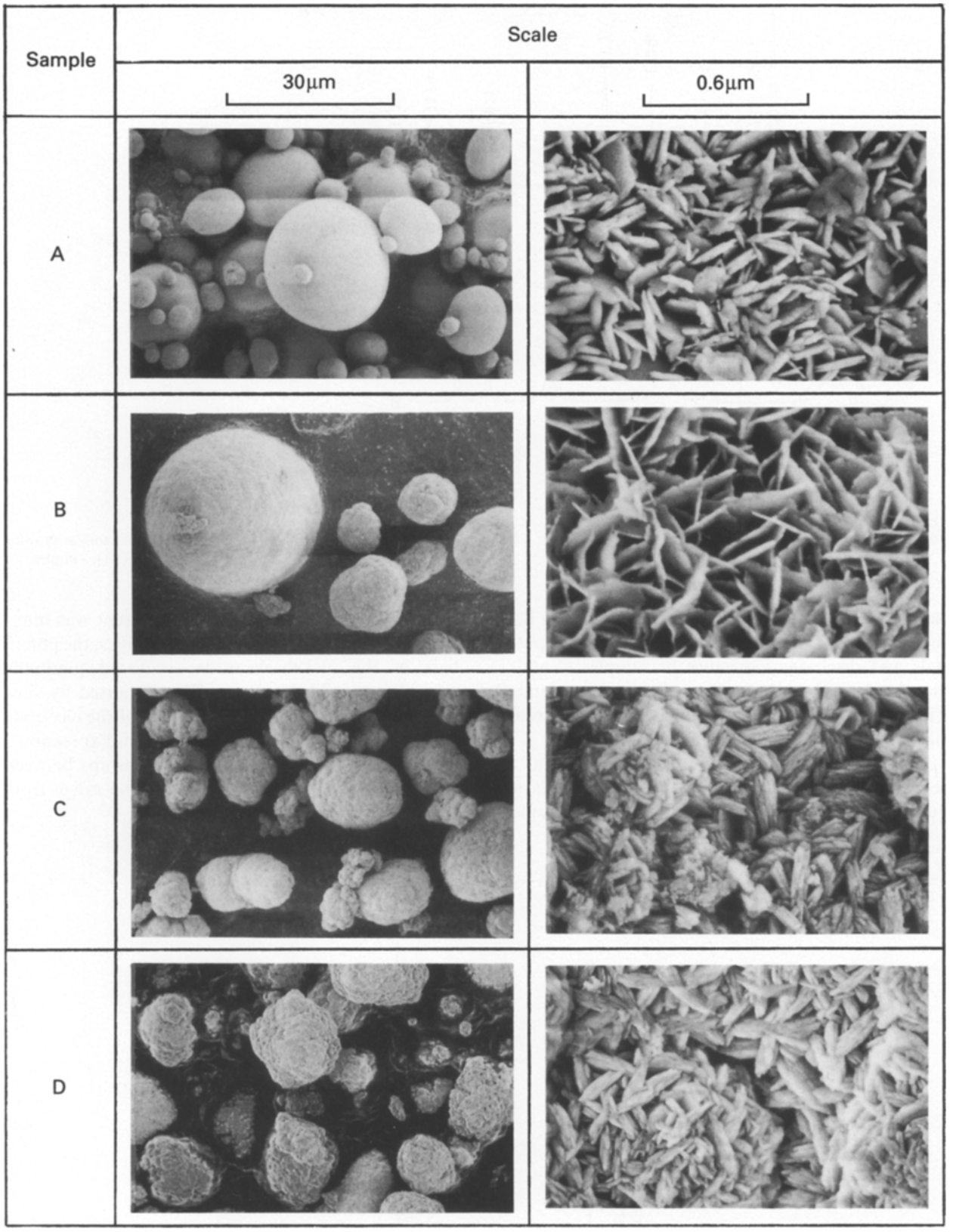

Fig. 1. SEM photograph of the samples.

with the result from XRD measurement (Table 2), that is, samples A and B, having larger crystalline size, show a higher decomposition temperature. Such a relationship between the decomposition temperature and the crystallite size of the nickel hydroxide sample were also observed by Fernandez Rodriguez *et al.* [7].

3.2. *Electrochemical characteristics of the nickel hydroxide electrode*

Initial charge and discharge curves of several nickel electrodes consisting of nickel hydroxide samples are shown in Fig. 4. It is found that the charging potential in sample A is higher than that of sample B, while

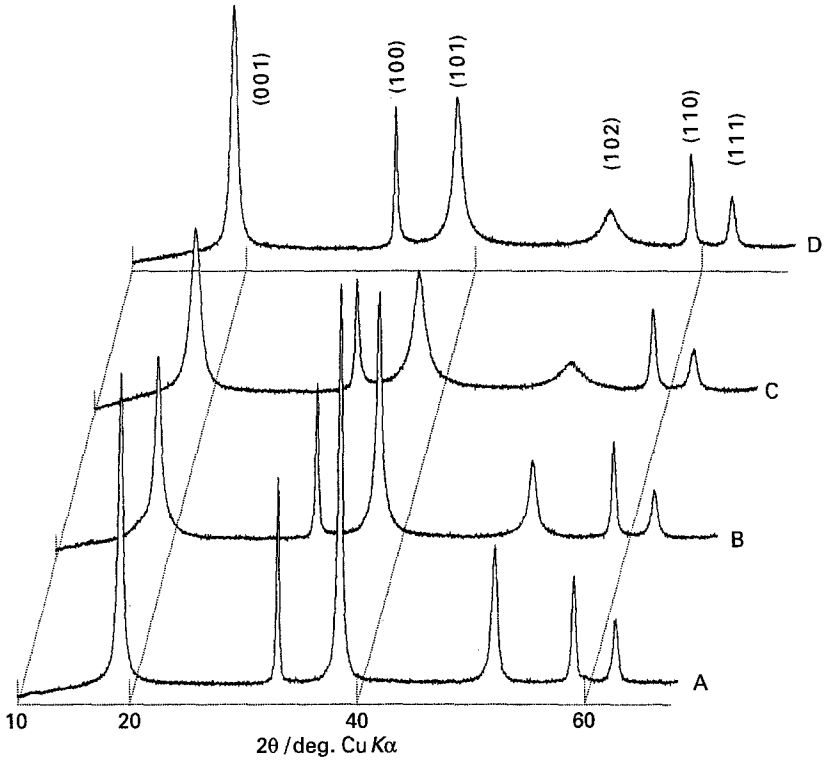

Fig. 2. XRD patterns of the samples showing the Miller indices of β-$Ni(OH)_2$ samples.

samples C and D have lower values than sample B. As seen from the discharge curves, the discharge potentials and discharge capacities of samples C and D are clearly higher than those of samples A and B. Thus, samples C and D with a smaller crystalline size, have better charge–discharge behaviour.

The open-circuit potentials were measured at the second discharge. The closed-circuit potentials and quasiequilibrium open-circuit potentials of sample C are presented in Fig. 5. When the current was interrupted after discharge to various capacities, the potentials of the nickel electrode recovered gradually toward an equilibrium state. This is caused by slow diffusion of protons from the surface of the electrode toward the bulk. The values of dE/dn in Expression 2 were obtained from the linear relationships between the o.c.v. and discharge capacity in the range from 50–200 mA h $(g\text{-}Ni(OH)_2)^{-1}$.

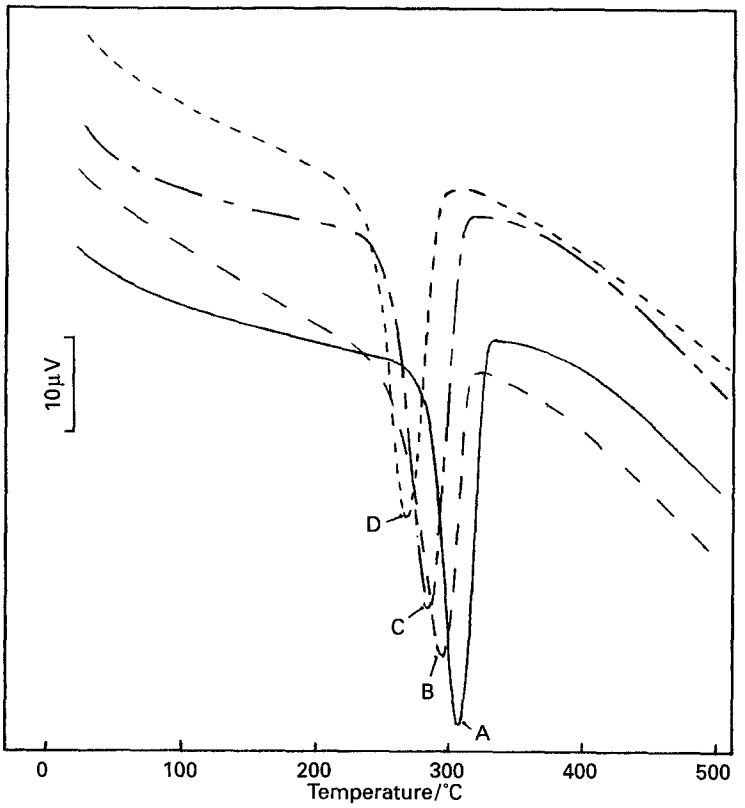

Fig. 3. DTA curves of the samples.

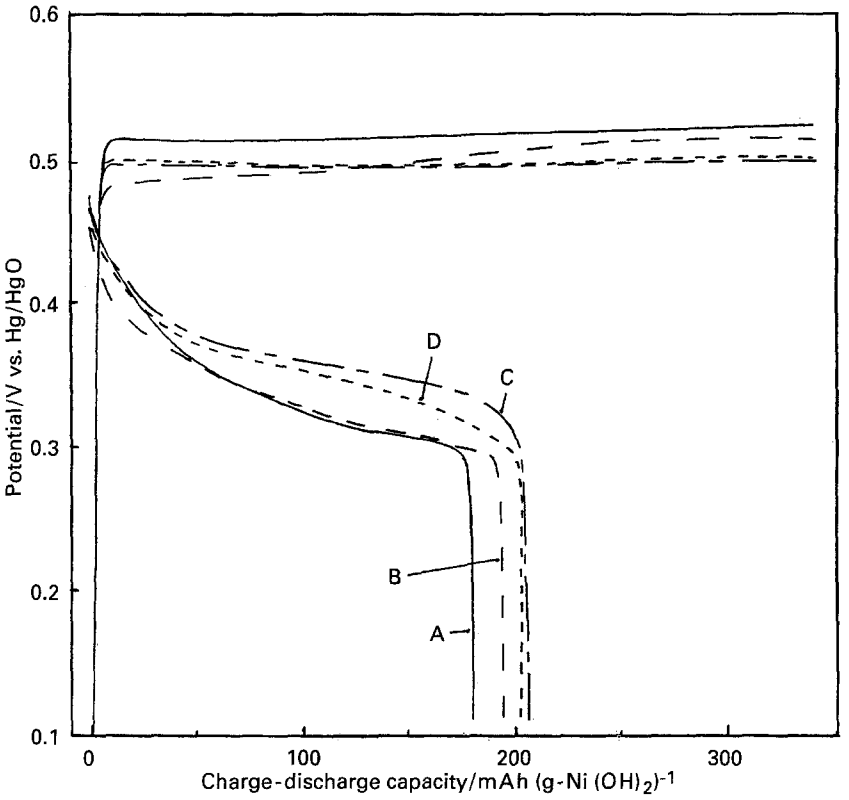

Fig. 4. Initial charge–discharge curves of the samples. Key: (——) A; (– – –) B; (– - –) C; (- - - -) D.

The diffusion of protons in nickel oxide was quantitatively investigated using the CPR techniques. A typical potential response during the passage and interruption of a constant current, I, for the sample C is shown as a function of time in Fig. 6(a), and the transient voltage (ΔE) observed after the passage of current pulse is plotted against $1/\sqrt{t}$ (Fig. 6(b)). In the initial period (0–40 s), the variation was not linear. This may be attributed to an 'electrolyte effect' caused by penetration of electrolyte into the porous electrode [4]. However, the $\Delta E/t$ relationship was found to be linear for the rest of the period (40–400 s). The slope of the linear region was used to calculate the chemical diffusion coefficient of the proton, $\tilde{D}$, in the nickel oxide using Expression 2.

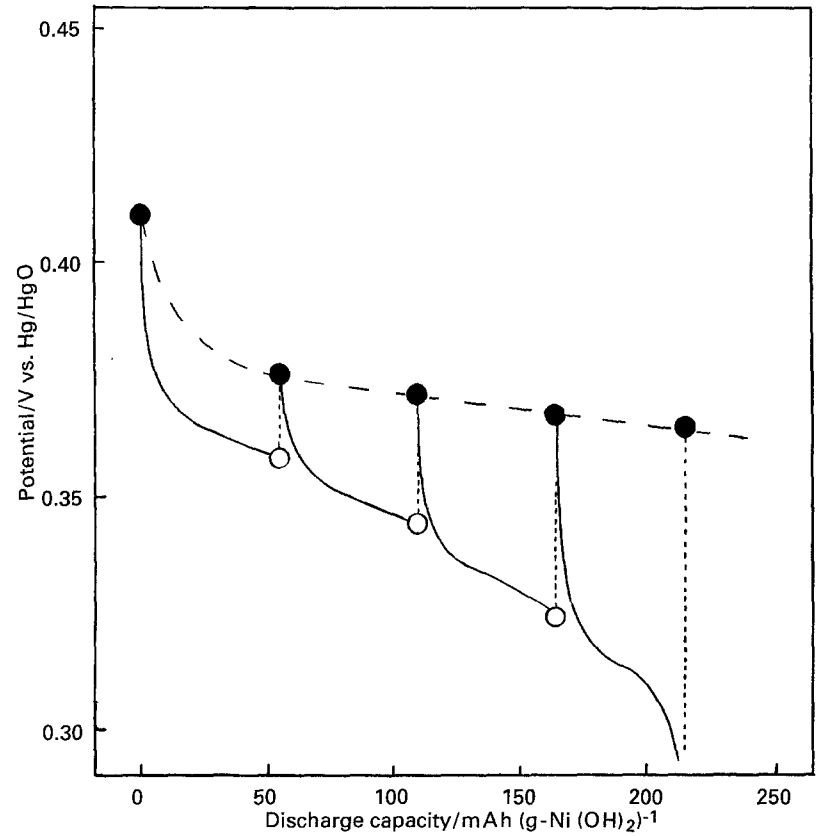

Fig. 5. Closed-circuit and open-circuit potentials as a function of discharge capacity of sample C at 20 °C. Key: (●) open-circuit potential; (○) closed-circuit potential; (- - - -) potential recovery after discharge. Discharge current density 7.0 mA cm^{-2}.

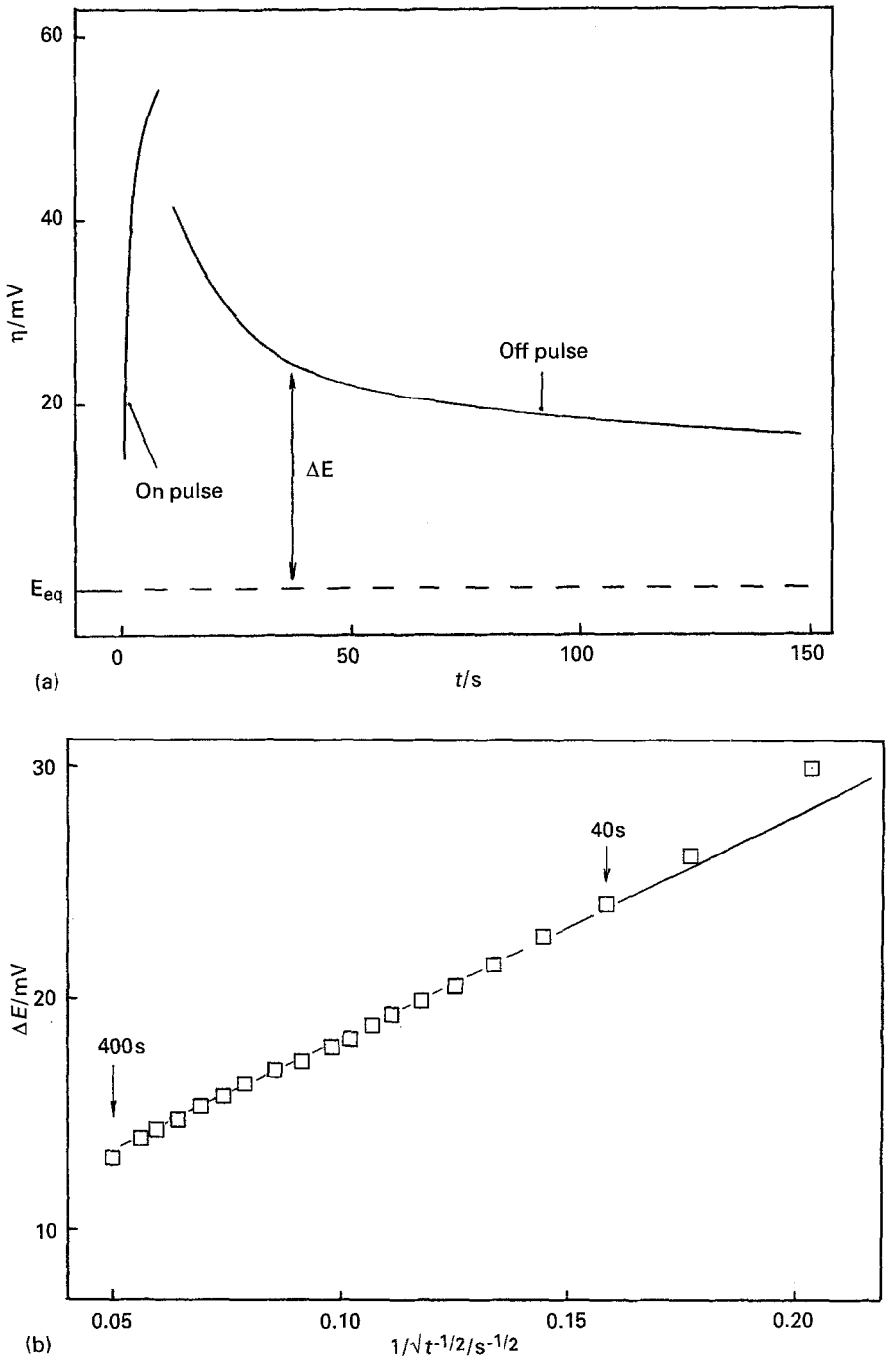

Fig. 6. (a) Typical potential response for sample C in current–pulse relaxation technique. E_{eq}, equilibrium potential before the passage of current pulse. (b) typical plot of observed voltage (ΔE) against $1/\sqrt{t}$ for sample C. Amplitude of current pulse, 300 mA; temperature, 20 °C.

The temperature dependence of $\tilde{D}$ in each sample is shown in Fig. 7. The $\tilde{D}$ values of the samples C and D are higher than that of the sample B, while that for sample A is lower than that for sample B. The value of $\tilde{D}$ cannot be extracted more accurately from the current pulse experiment because of the difficulty of estimating the effective surface area of the powder pressed electrode. In fact, the $\tilde{D}$ value in sample C obtained by using BET surface area ($38\,m^2\,g^{-1}$, Table 1) instead of geometric surface area was $2.22 \times 10^{-15}\,cm^2\,s^{-1}$ at 20 °C, which is significantly lower than that from geometric surface area ($4\,cm^2$) ($1.18 \times 10^{-10}\,cm^2\,s^{-1}$). However, as the charge and discharge processes do not seem to change the surface condition, the relative values of $\tilde{D}$ in Fig. 7 may reflect actual variations with temperature and the kinds of samples A ~ D.

From the slope of the lines in Fig. 7, the enthalpy (ΔH) and D_0 values for proton diffusion were obtained using the following equation:

$$\tilde{D} = D_0 \exp\left(-\frac{\Delta H}{RT}\right) \tag{5}$$

The values obtained are presented in Table 3. The ΔH values are similar in each sample, but the D_0 values of samples C and D are higher than that of sample B, while that in sample A is lower than that for sample B.

MacArthur has measured the proton diffusion coefficient in nickel hydroxide by the potential step technique [8]. He has reported a value of $\tilde{D} = 3.1 \times 10^{-10}\,cm^2\,s^{-1}$, $D_0 = 1.3 \times 10^{-8}\,cm^2\,s^{-1}$, $\Delta H = 0.095\,eV$ ($9.2 \times kJ\,mol^{-1}$) at 25 ~ 70 °C. These values are close to those for sample B (Table 3). Zhang *et al.* have measured the proton diffusion

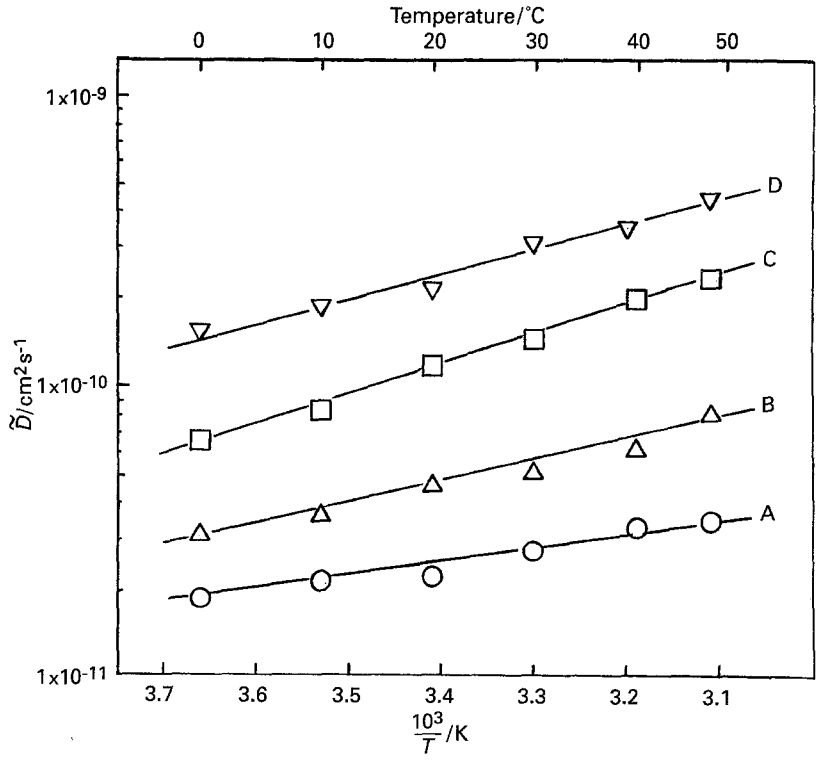

Fig. 7. Temperature dependence of proton diffusion coefficient for samples A–D.

coefficient in nickel hydroxide by cyclic voltammetric and chronoamperometic measurements and have reported $\tilde{D}$ values of $(5.0 \pm 0.6) \times 10^{-12}$ to $(10 \pm 3) \times 10^{-12}\,cm^2\,s^{-1}$ [9]. These values are considerably smaller than the present values (Fig. 7). The positive electrodes used by MacArthur [8] and Zhang *et al.* [9] were prepared by impregnation, but the present electrodes are pasted. Such a difference in preparation of the electrodes appears to result in different effective electrode areas, hence leading to considerable difference in the $\tilde{D}$ values.

β-$Ni(OH)_2$ has been characterized by X-ray diffraction [10] and EXAFS measurements [11]. The hydroxide has a brucite-type structure with a hexagonal unit cell having $a = 0.313$ nm, $c = 0.461$ nm. The crystal structure consists of stacked layers, each layer having a hexagonal arrangement of nickel atoms with octahedra of oxygen atoms. The stacking along the c-axis is weakly bound with van der Waals' forces.

Figure 8 shows a SEM photograph of sample C after two charge–discharge cycles (Fig. 4). This picture shows that the sample C consists of hexagonal plates, and the crystal form is maintained after repeated hydrogen insertion and deinsertion into and from the hexagonal structure.

Table 3. The ΔH and D_0 values for proton diffusion in nickel hydroxide samples

Sample	ΔH/eV	$D_0/cm^2\,s^{-1}$
A	0.0808	6.17×10^{-10}
B	0.140	1.21×10^{-8}
C	0.197	2.78×10^{-7}
D	0.167	1.82×10^{-7}

The electrode reaction accompanying proton diffusion in the hexagonal layers occurs as follows: $Ni(OH)_2 \rightleftharpoons NiOOH + H^+ + e^-$. The proton intercalation reaction occurs reversibly, while maintaining the hexagonal structure of nickel hydroxide. The hydroxide samples C and D, with a smaller crystalline size, showed a higher proton diffusion coefficient than samples A and B. This would diminish the concentration polarization of protons during discharge and recharge, leading to better charge–discharge behaviour, as observed in Figs 4 and 5. Thus, nickel hydroxide with a small crystalline size is suitable as an active material as a positive electrode in rechargeable alkaline batteries.

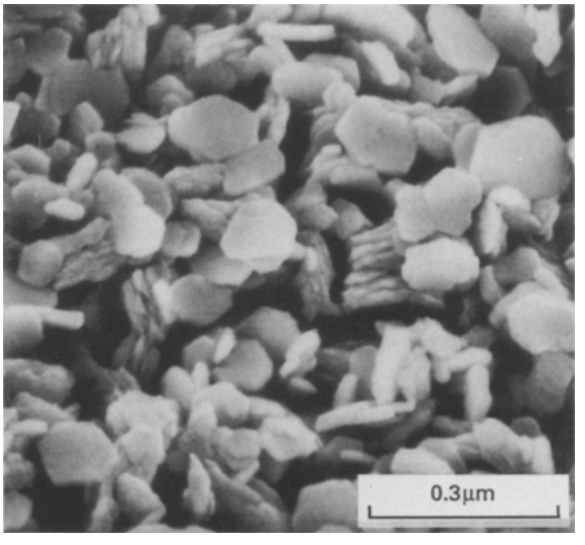

Fig. 8. SEM photograph of the sample C after charge–discharge cycles.

Acknowledgements

The authors thank K. Tamura and I. Aramaki for helpful suggestions and support.

References

[1] I. Matsumoto, M. Ikeyama, T. Iwaki and H. Ogawa, *Denki Kagaku* **54** (1986) 159.
[2] I. Matsumoto, M. Ikeyama, T. Iwaki, Y. Umeo and H. Ogawa, *ibid.* **54** (1986) 164.
[3] S. Basu and W. L. Worrell, Fast Ion Transport in Solids (edited by J. N. Mundy, P. D. Vashita and G. K. Shenoy), North-Holland, Amsterdam (1979) p. 149.
[4] N. Kumagai, S. Tanifuji, T. Fujiwara and K. Tanno, *Electrochim. Acta* **37** (1992) 1039.
[5] P. G. Dickens, S. J. Hibble and R. H. Jarman, *J. Electron. Mater.* **10** (1981) 999.
[6] B. D. Cullity, 'Elements of X-ray Diffraction', Addison-Wesley, Reading, MA (1956).
[7] J. M. Fernandez Rodriguez, J. Morales, J. L. Tirado, *J. Mater. Sci.* **21** (1986) 3668.
[8] D. M. MacArthur, *J. Electrochem. Soc.* **117** (1970) 729.
[9] C. Zhang and S. Park, *ibid* **134** (1987) 2966.
[10] P. Oliva, J. Leonardi, J. F. Laurent, C. Delmas, J. J. Braconnier, M. Figlarz, F. Fievet and A. Guibert, *J. Power Sources* **8** (1982) 229.
[11] K. I. Pandya, W. E. O'Grady, D. A. Corrigan, J. McBreen and R. W. Hohhman, *J. Phys. Chem.* **94** (1990) 21.